Stability of Contact Discontinuities in Electrostatic Hybrid- and Full-Vlasov Simulations

Naru TSUJINE, Takayuki HARUKI[1], Takayuki UMEDA[2], Yasuhiro NARIYUKI[3]
and Masahiro SATO[4]

Graduate School of Science and Engineering, University of Toyama, Toyama 930-8555, Japan
[1]*Faculty of Sustainable Design, Academic Assembly, University of Toyama, Toyama 930-8555, Japan*
[2]*Institute for Space-Earth Environmental Research, Nagoya University, Nagoya 464-8601, Japan*
[3]*Faculty of Education, Academic Assembly, University of Toyama, Toyama 930-8555, Japan*
[4]*Faculty of Engineering, Academic Assembly, University of Toyama, Toyama 930-8555, Japan*

The stability of contact discontinuities was studied by means of one-dimensional electrostatic (ES) hybrid- and full-Vlasov simulations with the initial parameter based on observational data. The ES hybrid-Vlasov simulations show that the sharp gradient of the ion number density is generated at the early stage and is subsequently maintained for a long term. On the other hand, the sharp gradient is absent in the ES full-Vlasov simulation. The generalized Ohm's law shows that the electron pressure gradient accounts for the electric field on the ion time scale in both ES hybrid- and full-Vlasov simulations. It is shown that there is a difference in the time evolution of the electron pressure between the ES hybrid- and full-Vlasov simulations, which is mainly caused by the electron heat flux.

1. Introduction

The contact discontinuity in magnetohydrodynamics is a boundary layer between different number densities and temperatures without a change of magnetic field and plasma flow velocity at uniform pressure [1]. The stability of boundary layers formed between two Maxwellian plasmas with different number densities and temperatures was discussed by means of kinetic simulations [2–5]. Wu *et al.* performed hybrid-particle-in-cell (PIC) simulations to study the stability of the boundary layer [2]. In hybrid simulations, ions and electrons are treated as superparticles and a fluid, respectively, and the charge neutrality is always satisfied. Their simulation results showed that a sharp gradient of the ion number density is maintained on the ion time scale, which is identified as a contact discontinuity. Lapenta and Brackbill have discussed the stability of the boundary layer by comparing the results between hybrid- and full-PIC simulations [3]. The behavior of electron pressure in the hybrid-PIC simulation is different from that in the full-PIC simulation because the hybrid simulation assumes the adiabatic law of the electron pressure. It was shown that a sharp gradient of the ion number density was not maintained in the full-PIC simulation.

Hsieh *et al.* have reported the evidence of contact discontinuities in the natural plasma from the in-situ observation by the Time History of Events and Macroscale Inter-

actions during Substorms (THEMIS) spacecraft [6]. It was shown that the length of the transition layer of contact discontinuities was estimated to be $\approx 4\rho_i$ to $12\rho_i$ (ρ_i is the ion gyroradius), which corresponds to several tens of the ion Debye length.

Tsai *et al.* have performed an electrostatic (ES) full-Vlasov simulation with various ion-to-electron temperature ratios [4]. They discussed the structures of number density and temperature without a jump in the total plasma pressure on the electron time scale. Later, Umeda *et al.* further performed ES full-Vlasov simulations with various temperature ratios [5]. They showed that the sharp gradient of ion number density is not maintained even on the electron time scale because the electric potential due to the charge separation is too small. This is consistent with the previous full-PIC simulation [3].

The parameters of contact discontinuities in the spacecraft observation ($T_{e1} / T_{i1} = 0.200$, $T_{e2} / T_{i2} = 0.304$ and $N_1 / N_2 = 0.73$) [6] differ from the initial parameters in the previous hybrid simulations ($T_{e1} / T_{e2} = T_{i1} / T_{i2} = 4$ and $N_1 / N_2 = 0.25$) [2, 3]. Here, subscripts 1 and 2 represent region 1 (low-density and high-temperature plasma) and region 2 (high-density and low-temperature plasma), respectively. In the previous hybrid simulations, the sharp gradient of ion number density was maintained on the ion time scale and was supported by the electric potential due to the electron pressure gradient [3]. The electron pressure

author's e-mail: d1771002@ems.u-toyama.ac.jp

is generally discussed by using the electron adiabatic law in hybrid simulations. Although the previous full-Vlasov simulation indicated the relationship between the electric potential and electron pressure [5], a sharp gradient of the ion number density was not maintained by the electric potential due to the charge separation in full-Vlasov simulations. Therefore, the time evolution of the electron pressure in hybrid- and full-Vlasov simulations is different.

In this study, we perform hybrid- and full-Vlasov simulations with the one-dimensional ES approximation by using the initial parameter based on the observational data. We adopt the ES approximation because the normal angle of magnetic fields is sufficiently small in the observational data ($\theta \approx 4°$ to $15°$) [6], and the sharp gradient of the ion number density is maintained for the long term without tangential magnetic fields in previous hybrid simulations [2]. We show that the electric field is supported by the electron pressure gradient in both hybrid- and full-Vlasov simulations by using the generalized Ohm's law. In addition, we clarify that there is a difference in the generation process of the electron pressure gradient between the hybrid- and full-Vlasov simulations by using the equation of the electron pressure.

We explain our two simulation models in Sec. 2. We compare the results of ES hybrid- and full-Vlasov simulations in Sec. 3. We summarize our conclusions in Sec. 4.

2. Simulation Model

We developed one-dimensional ES hybrid- and full-Vlasov codes to study contact discontinuities. The full-Vlasov simulation numerically solves both ion and electron motions by using phase-space distribution functions. On the other hand, in the hybrid-Vlasov simulation, unlike ions, electrons are solved numerically by using a fluid equation.

The Vlasov equation is described by

$$\frac{\partial f_s}{\partial t} + v\frac{\partial f_s}{\partial x} + \frac{q_s}{m_s}E\frac{\partial f_s}{\partial v} = 0, \tag{1}$$

where f, q, m, and E are the distribution function, charge, mass and electric field, respectively. Here, the subscript $s =$ e, i shows the species of ion and electron, respectively. The Vlasov equation is divided into two advection equations and is then solved by the splitting method [7]. These advection equations are numerically solved by the 4th-order conservative and non-oscillatory scheme, which satisfies the mass conservation, positivity, and non-oscillatory of the distribution function [8, 9].

In addition, the ES full-Vlasov model also solves Poisson's equation to obtain the electric field

$$\frac{\partial E}{\partial x} = \frac{\rho}{\epsilon_0}, \tag{2}$$

where ρ ($= q_iN_i + q_eN_e$) and ϵ_0 are the charge density and the permittivity in vacuum, respectively. On the other hand, the evaluation of the electric field is different from

Eq. (2) in the hybrid-Vlasov model because of the charge neutrality ($\rho = 0$). To evaluate the electric field, the generalized Ohm's law is derived by coupling ion and electron Vlasov equations,

$$\left(\frac{q_i^2}{m_i}N_i + \frac{q_e^2}{m_e}N_e\right)E = \frac{\partial J}{\partial t} + q_i\frac{\partial}{\partial x}\left(N_iU_i^2 + \frac{1}{m_i}P_i\right)$$
$$+ q_e\frac{\partial}{\partial x}\left(N_eU_e^2 + \frac{1}{m_e}P_e\right), \tag{3}$$

which is used in hybrid simulations [10, 11]. Here, J ($= q_iN_iU_i + q_eN_eU_e$) is the current density. It is noted that the $U_s\times B$ and $\nabla\times\nabla\times E$ terms are absent in Eq. (3) because of the one-dimensional ES approximation [11]. Here, the number density N, bulk velocity U, and pressure P are obtained by taking the moments of the distribution function,

$$N_s = \int_{-\infty}^{\infty} f_s dv, \tag{4}$$

$$U_s = \frac{1}{N_s}\int_{-\infty}^{\infty} vf_s dv, \tag{5}$$

$$P_s = m_s\int_{-\infty}^{\infty} (v - U_s)^2 f_s dv. \tag{6}$$

In the hybrid simulation, the electron number density and bulk velocity are equal to the ion number density and bulk velocity, respectively, due to the charge neutrality. This means that the time differential of the current density in Eq. (3) is always zero. The number density and momentum conservation laws for electrons are not solved in the hybrid simulation due to $N_e = N_i$ and $U_e = U_i$.

Wu *et al.* have solved the electron pressure by using the following energy equation with a convective term [2]

$$\frac{\partial}{\partial t}\left(\frac{P_e}{N_e^{\gamma_e}}\right) + U_e\frac{\partial}{\partial x}\left(\frac{P_e}{N_e^{\gamma_e}}\right) = 0, \tag{7}$$

where γ is a specific heat ratio. On the other hand, Lapenta and Brackbill ignored the convective term in Eq. (7) because they described that there was a small difference in the results with or without the convective term [3]. It is well known that the time differential of the electron pressure is also obtained from Eq. (7) as

$$\frac{\partial P_e}{\partial t} = -\frac{\partial}{\partial x}(P_eU_e) - (\gamma_e - 1)P_e\frac{\partial U_e}{\partial x}. \tag{8}$$

We confirmed that the hybrid-Vlasov simulations by using Eq. (7) with or without the convective term and by using Eq. (8) gave almost the same results. Therefore, we show the results by using Eq. (8) only.

The initial condition is identical to the previous ES full-Vlasov simulation [5]. Two Maxwellian plasmas with different number densities and temperatures but the same total plasma pressure across the boundary layer are initially set in this simulations. To express the jump in the discontinuity, the number density and the electron to ion temper-

ature ratio are described by a form of the tanh function,

$$N = \frac{N_2 - N_1}{2} \tanh\left(\frac{x}{\lambda}\right) + \frac{N_2 + N_1}{2}, \quad (9)$$

$$\frac{T_e}{T_i} = \frac{\frac{T_{e2}}{T_{i2}} - \frac{T_{e1}}{T_{i1}}}{2} \tanh\left(\frac{x}{\lambda}\right) + \frac{\frac{T_{e2}}{T_{i2}} + \frac{T_{e1}}{T_{i1}}}{2}, \quad (10)$$

where λ is the length of the transition layer. The initial total plasma pressure P_0 ($= N_e T_e + N_i T_i$) (here, the Boltzmann constant is omitted) is uniform along the x direction. Therefore, the electron and ion pressures are obtained by

$$P_e = \frac{P_0\left[(T_{e2}T_{i1} - T_{e1}T_{i2})\tanh\left(\frac{x}{\lambda}\right) + T_{e2}T_{i1} + T_{e1}T_{i2}\right]}{(T_{e2}T_{i1} - T_{e1}T_{i2})\tanh\left(\frac{x}{\lambda}\right) + T_{e2}T_{i1} + T_{e1}T_{i2} + 2T_{i2}T_{i1}}, \quad (11)$$

$$P_i = \frac{2P_0 T_{i2}T_{i1}}{(T_{e2}T_{i1} - T_{e1}T_{i2})\tanh\left(\frac{x}{\lambda}\right) + T_{e2}T_{i1} + T_{e1}T_{i2} + 2T_{i2}T_{i1}}. \quad (12)$$

The ion to electron mass ratio is $m_i / m_e = 1836$. The electron to ion temperature ratio in regions 1 and 2 are $T_{e1} / T_{i1} = 0.200$ and $T_{e2} / T_{i2} = 0.304$, respectively. Similarly, the electron temperature ratio of regions 1 to 2 is $T_{e1} / T_{e2} = 0.983$. The number density ratio of regions 1 to 2 is $N_1 / N_2 = 0.73$. Note that these parameters are based on the observational data by the THEMIS spacecraft [6]. We take the spatial and velocity grid numbers as $N_x = 12,000$ and $N_v = 1000$, respectively. The spacing of the spatial grids is $\Delta x = 0.27\lambda_{Di2} = 0.5\lambda_{De2}$. The spacings of the electron and ion velocity grids are $\Delta v_e = 0.032 v_{the2}$ and $\Delta v_i = 0.152 v_{thi2}$, respectively. The permittivity in vacuum is set to be unity. The initial half thickness of the transition layer is $\lambda = 1.1\lambda_{Di2} = 2\lambda_{De2}$. It is known that γ_e is generally 3 in the one-dimensional ES approximation, which is used in this hybrid-Vlasov simulation. We determine that $\gamma_e \propto \log(P_e / N_e)$ is almost unity in the full-Vlasov simulation with the present initial parameter. Therefore, we also perform an additional hybrid-Vlasov simulation with $\gamma_e = 1$. The time step is set as $\Delta t = 0.025 / \omega_{pe2}$. It is noted that we use these completely the same initial parameters for the hybrid- and full-Vlasov simulations because of the direct comparison.

The continuous boundary condition is imposed in the x direction ($\partial / \partial_x = 0$), while the open boundary condition is imposed in the v_x direction. It is known that non-physical and numerical oscillations are generated due to the DC component of the electric field in one-dimensional simulation [12]. We perform the full-Vlasov simulation without the DC component of the electric field to remove the non-physical oscillations.

3. Simulation Results

We compare the time evolution of discontinuous boundary layers between the ES hybrid- and full-Vlasov

simulations. All of the physical quantities used in these simulations are normalized by the values in region 2 (high-density and low-temperature region). For instance, the time and spatial length are normalized by an electron plasma frequency ω_{pe2} and Debye length λ_{De2}, respectively. The notations of ($\gamma_e = 3$) and ($\gamma_e = 1$) mean the hybrid simulations with $\gamma_e = 3$ and 1, respectively.

Figure 1 shows the spatial profiles of the ion number density and electric field at $\omega_{pe2}t = 40, 100, 1000$ and 5000 in the ES hybrid- and full-Vlasov simulations. We determined that in these simulations, the transition layer of ion number density becomes wider as the time advances. A sharp gradient of the ion density is generated inside the transition layer in the hybrid-Vlasov simulations. On the other hand, this sharp gradient of the ion density is not found in the full-Vlasov simulation. Compared with the full-Vlasov simulation, the time evolution of the ion number density is similar except for the existence of a sharp gradient near the $x / \lambda_{De2} = 0$ in the hybrid-Vlasov simulations. The structure of the sharp gradient with $\gamma_e = 3$ is different from that with $\gamma_e = 1$. The sharp gradient of the ion number density is maintained for the long term without tangential magnetic fields, which is consistent with the previous hybrid-PIC simulation [2].

A positive peak of the electric field is observed inside the transition layer in the hybrid-Vlasov simulations, as seen in the spatial profiles of the electric field in Fig. 1. However, this peak is not observed in the full-Vlasov simulation. We determined that the positive peaks of the electric field are generated at an early stage ($\omega_{pe2}t \leq 100$) in the hybrid-Vlasov simulations, and then, their intensities increase with time. In addition, we also observed that the intensity of the positive peak with $\gamma_e = 3$ is larger than that with $\gamma_e = 1$. The result suggests that the positive peak of the electric field maintains a sharp gradient of ion number density.

We introduce the generalized Ohm's law [see Eq. (3)] to analyze the positive peak of the electric field in the transition layer. We confirmed that the two terms whose factor is $1 / m_i$ are sufficiently small and the two terms, including bulk velocities, do not contribute to the electric field formation because both electron and ion bulk velocities are sufficiently smaller than the electron thermal velocity. Hence, we focus on two terms $E_{P_e} \propto \partial P_e / \partial x$ and $E_J \propto \partial J / \partial t$ in Eq. (3). The term $\partial J / \partial t$ disappears in the hybrid-Vlasov simulations because of the charge neutrality.

Figure 2 shows the spatial profiles of the two terms in the generalized Ohm's law at $\omega_{pe2}t = 40, 100, 1000$ and 5000 in the ES hybrid- and full-Vlasov simualtions. As shown in Fig. 1, the electric field is over-plotted by red circles. Because the blue solid line agrees well with the red circles, the electron pressure gradient supports the electric field in the hybrid-Vlasov simulations with both $\gamma_e = 3$ and 1. On the other hand, the electric field is supported by both the electron pressure gradient and time differential of the current density in the full-Vlasov simulation. Note that
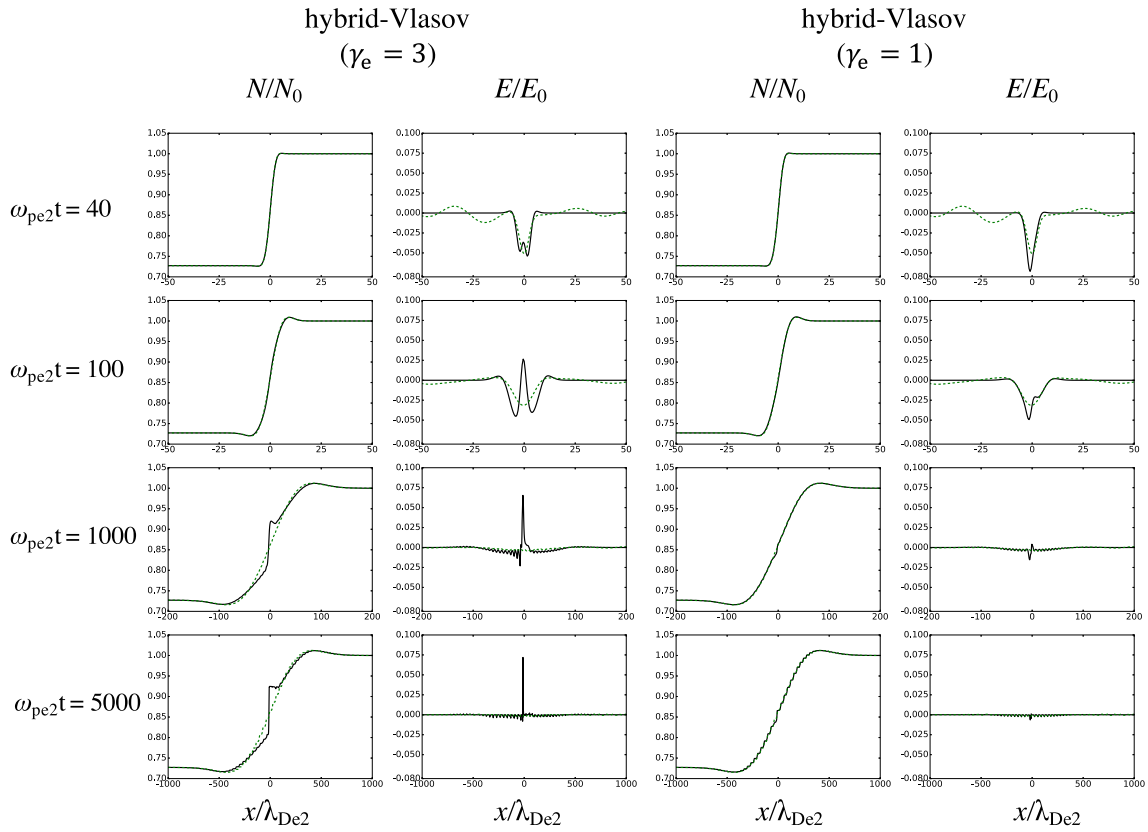
Fig. 1 Spatial profiles of the ion number density and electric field at $\omega_{pe2}t = 40, 100, 1000$ and 5000 in the ES hybrid- and full-Vlasov simulations. The hybrid- and full-Vlasov simulation results are plotted as black solid and green dashed lines, respectively. The number density and electric field are normalized by $N_0 \; (= N_2)$ and $E_0 \left(= m_e \omega_{pe2} v_{the2} \, / \, q_e\right)$, respectively.
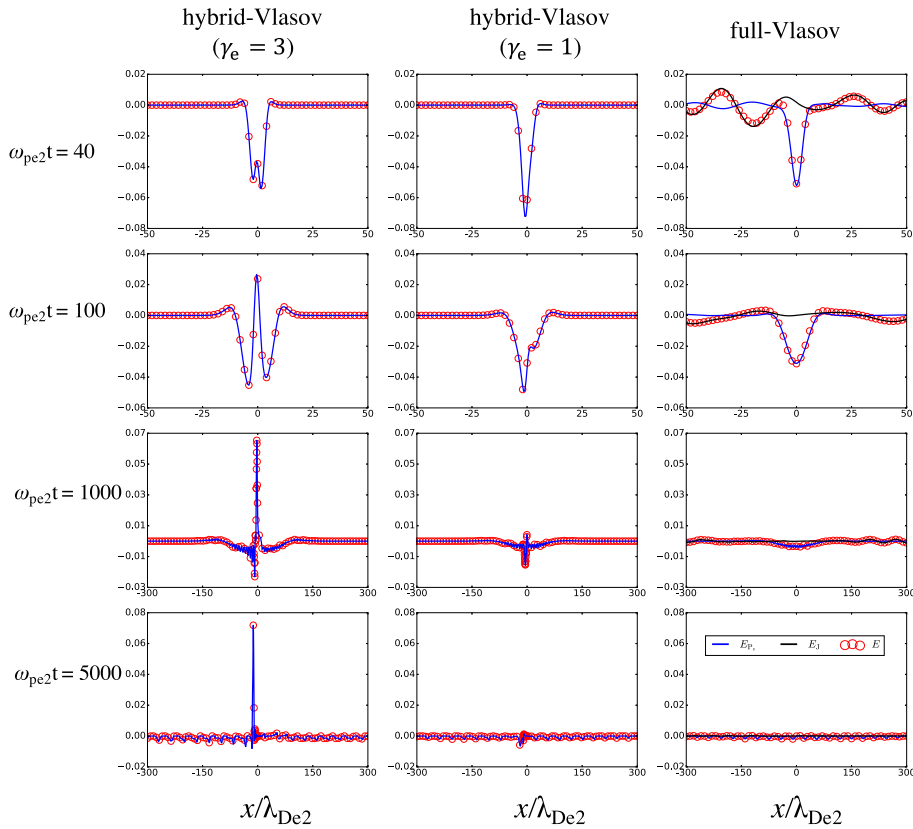

Fig. 2 Spatial profiles of the two terms in the generalized Ohm's law at $\omega_{pe2}t = 40, 100, 1000$ and 5000 in the ES hybrid- and full-Vlasov simulations. The gradient of electron pressure and time differential of the current density are plotted as blue and black solid lines, respectively. The electric field shown in Fig. 1 is over-plotted by red circles. These terms are normalized by E_0.
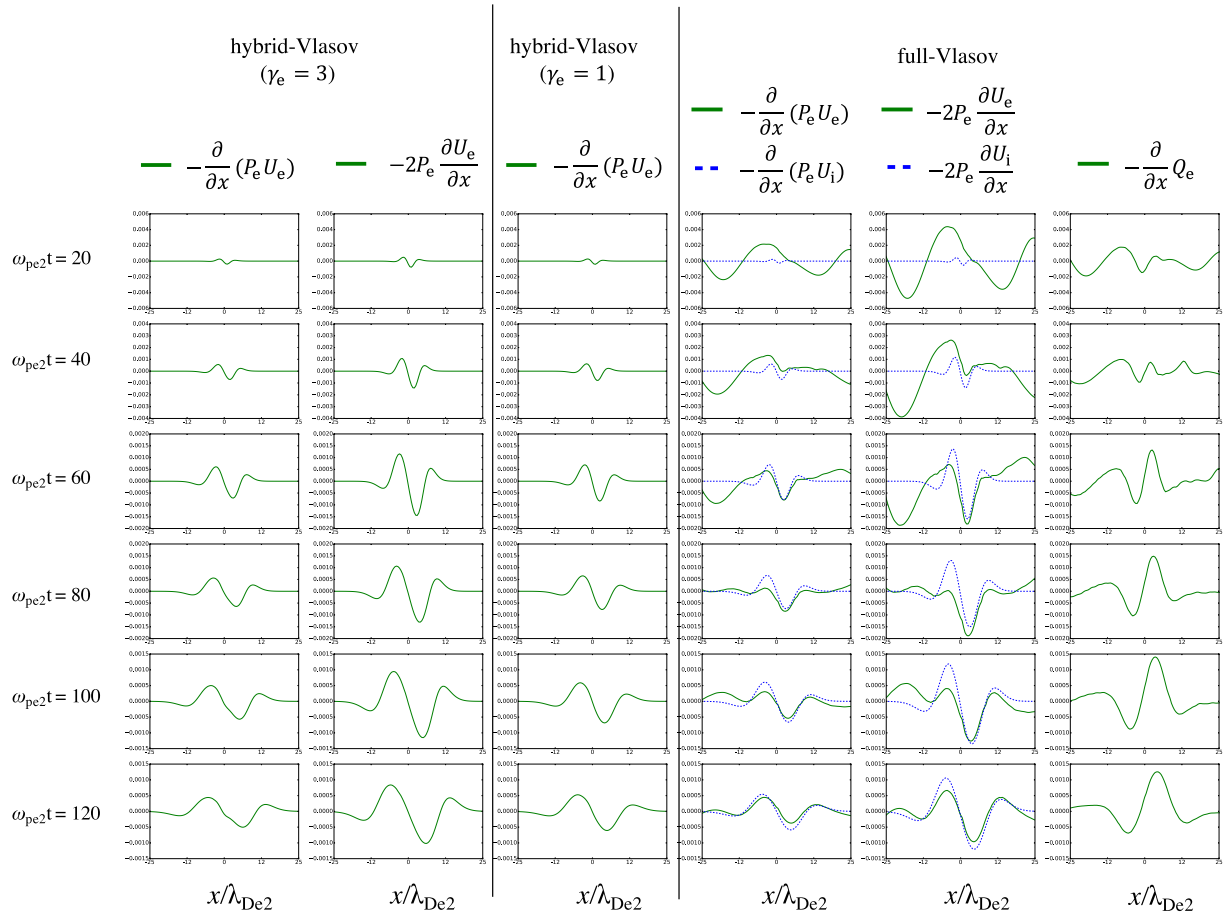
Fig. 3   Spatial profiles of electron advection, compression and heat flux terms at $\omega_{pe2}t = 20$, 40, 80, 100 and 120 in the ES hybrid- and full-Vlasov simulations. The green solid and blue dashed lines show the terms associated with electron and ions, respectively.

the relationship between the electron pressure gradient and electric field associated with the electrostatic potential was pointed out in the previous full-Vlasov simulation [5]. The time differential of the current density contributes electric field on the electron time scale in the full-Vlasov simulation. Hence, this term is ignored in this analysis. The positive peaks of the electric field due to the electron pressure are already generated at $\omega_{pe2}t = 40$ with $\gamma_e = 3$ and $\omega_{pe2}t = 100$ with $\gamma_e = 1$, respectively, and then evolve in time in the hybrid-Vlasov simulations. In this study, it is confirmed that the electron pressure gradient plays a major role in the electric field on the ion time scale in both hybrid- and full-simulations, although the structure of the electron pressure gradient in these simulations is different.

Because the peaks of the electric field are formed at the early stage ($\omega_{pe2} \leq 100$), we introduce the following equation for the time evolution of the electron pressure with a heat flux

$$\frac{\partial P_e}{\partial t} = -\frac{\partial}{\partial x}(P_e U_e) - (\gamma_e - 1) P_e \frac{\partial U_e}{\partial x} - \frac{\partial Q_e}{\partial x}, \quad (13)$$

which is related to the electric field. Here, the heat flux is defined as

$$Q_s = \int_{-\infty}^{\infty} m_s (v - U_s)^3 f_s dv. \quad (14)$$

Note that we omitted the discussion on the time evolution of the ion pressure at the early stage because the ion pressure does not contribute in Eq. (3) due to the large ion mass m_i.

Figure 3 shows the spatial profiles of electron advection, compression, and heat flux terms at $\omega_{pe2}t = 20$, 40, 80, 100, and 120 in the ES hybrid- and full-Vlasov simulations. In the hybrid-Vlasov simulations, the conditions $N_e = N_i$ and $U_e = U_i$ are imposed due to the charge neutrality, and the electron heat flux is always zero ($Q_e = 0$) due to the adiabatic process. On the other hand, the electron heat flux term in the full-Vlasov simulation is calculated by Eq. (14) with the electron velocity distribution function. It is known that Eq. (13) with $\gamma_e = 3$ corresponds to the second moment of the Vlasov Eq. (1). Hence, we set the electron specific heat ratio $\gamma_e = 3$ to analyze the full-Vlasov simulation result.

The advection and compression terms in the hybrid-Vlasov simulations are similar to the terms associated with *ions* in the full-Vlasov simulation. On the other hand, these terms in the hybrid-Vlasov simulations are different from those associated with *electrons* in the full-Vlasov simulation at the early stage ($\omega_{pe2}t \leq 100$). The advection, compression and heat flux terms associated with electrons be-

come steady on the electron time scale in the full-Vlasov simulation, which may affect ion profiles.

In the hybrid-Vlasov simulation with $\gamma_e = 1$, the advection term in Eq. (13) is described by using the charge conservation law $\partial \rho / \partial t = -\partial J / \partial x = -\partial / \partial x (q_i N_i U_i) - \partial / \partial x (q_e N_e U_e)$ as

$$\frac{\partial}{\partial x}(P_e U_e) \approx T_e \frac{\partial}{\partial x}(N_e U_e)$$
$$= -\frac{T_e}{e}\frac{\partial \rho}{\partial t} - T_e \frac{\partial}{\partial x}(N_i U_i), \qquad (15)$$

where e is the elemental charge. Equation (15) suggests that the time evolution of the charge density, which is ignored in the hybrid-Vlasov simulations, affects the time evolution of the electron pressure. The difference in the ion number density between the hybrid-Vlasov simulation with $\gamma_e = 1$ and full-Vlasov simulation is caused by the charge separation.

The electron heat flux term cancels the compression term for $\omega_{pe2}t \geq 120$ in the full-Vlasov simulation, which makes the full-Vlasov system isothermal. This is consistent with $\gamma_e \propto \log(P_e / N_e) \approx 1$ in the full-Vlasov simulation (see Sec. 2). In the hybrid-Vlasov simulation with $\gamma_e = 3$, the intensity of the compression term, which is canceled by the electron heat flux term in the full-Vlasov simulation, is larger than that of the advection term. These results suggest that the electron heat flux plays an important role in the time evolution of the electron pressure. It should be noted that we performed additional simulations that solve the momentum conservation law of electrons only or both the number density and momentum conservation laws of electrons in the hybrid model. In these simulations, the sharp gradient of the ion number density is observed, as seen in Fig. 1, which also suggests that the electron heat flux has a greater impact than that of the charge density.

4. Conclusions

Previous studies have shown that a sharp gradient of the ion number density formed between two Maxwellian plasmas with different number densities and temperatures was maintained in the hybrid simulations but was relaxed in the full-kinetic simulations [2, 3, 5]. In this study, the direct comparison between the ES hybrid- and full-Vlasov simulations was made with the same initial parameter based on the observational data.

Our conclusions are summarized below.

1. A sharp gradient of the ion number density is formed inside the transition layer on the ion time scale ($\omega_{pi2}t > 100$) in the ES hybrid-Vlasov simulations with both $\gamma_e = 3$ and 1. This is consistent with the

previous studies [2, 3].

2. The electric field on the ion time scale is supported by the electron pressure gradient in the generalized Ohm's law in both hybrid- and full-Vlasov simulations. In the ES hybrid-Vlasov simulations, the positive peak of the electron pressure gradient associated with the sharp gradient of ion number density is generated on the electron time scale ($\omega_{pe2}t \leq 100$).

3. The electron heat flux and the charge density affect the time evolution of the electron pressure in the full-Vlasov simulation. The electron heat flux plays an important role in making a difference between the full- and hybrid-Vlasov simulations by canceling the compression term.

It is noted that two Maxwellian distributions with non-uniform temperature do not have equilibrium in the Vlasov-Poisson system as shown in the previous study [5]. The THEMIS observation of the stable structure of the transition layer with a spatial scale of several tens of the ion Debye length cannot be explained by the present simulation model. Therefore, a Vlasov-Poisson equilibrium with non-Maxwellian distributions is left as a future study for the stable structure of the contact discontinuity.

[1] W. Baumjohann and R.A. Treumann, *Basic Space Plasma Physics* (Imperial College Press, 1996).
[2] B.H. Wu, J.K. Chao, W.H. Tsai, Y. Lin and L.C. Lee, Geophys. Res. Lett. **21**, 2059 (1994).
[3] G. Lapenta and J.U. Brackbill, Geophys. Res. Lett. **23**, 1713 (1996).
[4] T.C. Tsai, L.H. Lyu, J.K. Chao, M.Q. Chen and W.H. Tsai, J. Geophys. Res. **114**, A12103 (2009).
[5] T. Umeda, N. Tsujine and Y. Nariyuki, Phys. Plasmas **26**, 102107 (2019).
[6] W.C. Hsieh, J.H. Shue, J.K. Chao, T.C. Tsai, Z. Nemecek and J. Safrankova, Geophys. Res. Lett. **41**, 8228 (2014).
[7] C.Z. Cheng and G. Knorr, J. Comput. Phys. **22**, 330 (1976).
[8] T. Umeda, Earth, Planets Space **60**, 773 (2008).
[9] T. Umeda, Y. Nariyuki and D. Kariya, Comput. Phys. commun. **183**, 1094 (2012).
[10] F. Valentini, P. Trávníček, F. Califano, P. Hellinger and A. Mangeney, J. Comput. Phys. **225**, 753 (2007).
[11] T. Amano, J. Comput. Phys. **366**, 366 (2018).
[12] Y. Omura and H. Matsumoto, *Computer Space Plasma Physics: Simulation Techniques and Software*, edited by H. Matsumoto and Y. Omura (Terra Scientific, 1993).